The EMBO Journal (2011) 30, 2920–2933 | © 2011 European Molecular Biology Organization | All Rights Reserved 0261-4189/11
www.embojournal.org

THE EMBO JOURNAL

FLRT2 and FLRT3 act as repulsive guidance cues for Unc5-positive neurons

Satoru Yamagishi[1,7,8], Falko Hampel[1,8], Katsuhiko Hata[2], Daniel del Toro[1], Manuela Schwark[3,4], Elena Kvachnina[3], Martin Bastmeyer[5], Toshihide Yamashita[2], Victor Tarabykin[3,4], Rüdiger Klein[1,*] and Joaquim Egea[1,6,*]

[1]Department of Molecular Neurobiology, Max Planck Institute of Neurobiology, Am Klopferspitz, Martinsried, Germany, [2]Department of Molecular Neuroscience, Osaka University Graduate School of Medicine, Osaka, Japan, [3]Max Planck Institute for Experimental Medicine, Hermann-Rein Strasse, Göttingen, Germany, [4]Neurocure Exzellenzcluster, Institute of Cell Biology and Neurobiology, Charité-Universitätsmedizin Berlin, Campus Mitte, Berlin, Germany, [5]Karlsruher Institut für Technologie (KIT), Zoologisches Institut Abteilung für Zell- und Neurobiologie, Haid-und-Neu-Strasse, Karlsruhe, Germany and [6]Departament de Ciències Mèdiques Bàsiques, Facultat de Medicina, Universitat de Lleida/IRBLLEIDA, Spain

Netrin-1 induces repulsive axon guidance by binding to the mammalian Unc5 receptor family (Unc5A–Unc5D). Mouse genetic analysis of selected members of the Unc5 family, however, revealed essential functions independent of Netrin-1, suggesting the presence of other ligands. Unc5B was recently shown to bind fibronectin and leucine-rich transmembrane protein-3 (FLRT3), although the relevance of this interaction for nervous system development remained unclear. Here, we show that the related Unc5D receptor binds specifically to another FLRT protein, FLRT2. During development, FLRT2/3 ectodomains (ECDs) are shed from neurons and act as repulsive guidance molecules for axons and somata of Unc5-positive neurons. In the developing mammalian neocortex, Unc5D is expressed by neurons in the subventricular zone (SVZ), which display delayed migration to the FLRT2-expressing cortical plate (CP). Deletion of either FLRT2 or Unc5D causes a subset of SVZ-derived neurons to prematurely migrate towards the CP, whereas overexpression of Unc5D has opposite effects. Hence, the shed FLRT2 and FLRT3 ECDs represent a novel family of chemorepellents for Unc5-positive neurons and FLRT2/Unc5D signalling modulates cortical neuron migration.
The EMBO Journal (2011) **30,** 2920–2933. doi:10.1038/emboj.2011.189; Published online 14 June 2011

*Corresponding author. R Klein, Department of Molecular Neurobiology, Max Planck Institute of Neurobiology, Am Klopferspitz 18, Martinsried 82152, Germany. Tel.: +49 898 578 3150; Fax: +49 898 578 3152; E-mail: rklein@neuro.mpg.de or J Egea, Departament de Ciencies Mediques Basiques, Facultat de Medicina, Universitat de Lleida/IRBLLEIDA, Montserrat Roig 2, Lleida 25198, Spain. Tel.: +34 973 70 22 87; Fax: +34 973 70 24 26; E-mail: joaquim.egea@cmb.udl.es
[7]Present address: Department of Anatomy and Neuroscience, Hamamatsu University School of Medicine, Shizuoka 431-3192, Japan
[8]These authors contributed equally to this work

Received: 15 December 2010; accepted: 20 May 2011; published online: 14 June 2011

Subject Categories: neuroscience
Keywords: cell migration; cortex development; FLRT; repulsive guidance; Unc5

Introduction

Migrating cells and pathfinding axons are guided by molecular cues within the extracellular matrix or on the surface of ambient cells. These cues are interpreted as attractive or repulsive, depending on the set of receptors and signal transducers the cell expresses. The mammalian Unc5 receptor family comprises four orthologues (Unc5A–Unc5D), which function as repulsive axon-guidance receptors for Netrin (Leonardo *et al*, 1997; Moore *et al*, 2007) and RGMa (Bradford *et al*, 2009; Hata *et al*, 2009). The role of Unc5 protein in axon guidance has been clearly demonstrated in several model organisms (Mehlen and Furne, 2005) and more recent work has implicated Netrin/Unc5 signalling in angiogenesis and cell survival (Mehlen and Furne, 2005; Bradford *et al*, 2009). Genetic ablation of Unc5C leads to several CNS phenotypes including aberrant migration of cerebellar granule and Purkinje cells, and motor axon guidance defects (Ackerman *et al*, 1997; Burgess *et al*, 2006). Interestingly, these functions were not seen in *Netrin-1*$^{-/-}$ mice, indicating the participation of other Netrins (Moore *et al*, 2007) or other unrelated ligands for the Unc5 receptor family (Burgess *et al*, 2006).

Unc5B and Unc5D have recently been shown to bind with high affinity to the ectodomain (ECD) of fibronectin and leucine-rich transmembrane protein-3 (FLRT3) (Karaulanov *et al*, 2009; Sollner and Wright, 2009), a transmembrane protein that is thought to act cell autonomously either as a co-receptor or as a cell adhesion molecule in early embryogenesis (Bottcher *et al*, 2004; Karaulanov *et al*, 2006; Egea *et al*, 2008; Maretto *et al*, 2008). The Unc5B/FLRT3 complex regulates cell adhesion through the Rho small GTPase Rnd1 (Ogata *et al*, 2007; Karaulanov *et al*, 2009), but its role in neural development is unknown. Other *ex vivo* studies have shown that FLRT3 promotes neurite growth non-cell autonomously (Tsuji *et al*, 2004) or cell autonomously (Robinson *et al*, 2004). The related FLRT2 protein is essential for heart development (Muller *et al*, 2011), while the function of FLRT1 has not been explored.

Unc5D has recently been shown to be expressed by multipolar cells, which are the progeny of a population of cortical precursor cells, the so-called intermediate or basal progenitor cells (BPs), which populate the subventricular zone (SVZ) (Sasaki *et al*, 2008). BPs can be considered to be neurogenic transit amplifying progenitors that expand the pool of differentiated neuronal cells. This process contrasts with neuronal generation directly from apical progenitors, which are located in the ventricular zone (VZ). Both kinds of proliferative progenitors give rise to cortical projection neurons, which form the mammalian cerebral cortex. Projection neurons are produced in a temporal sequence

and undergo radial migration to reach their final laminar positions. Radial migration follows an 'inside–out' pattern such that later born neurons trespass older neurons and occupy more superficial positions in the neocortex (Rakic, 1988).

This 'inside–out' rule, however, is not respected by all cortical neurons. Neurons that express Unc5D (Sasaki *et al*, 2008) and the SVZ marker Svet1 (Tarabykin *et al*, 2001), which comprises a non-coding RNA encoded by an intronic region of the unspliced RNA of Unc5D (Sasaki *et al*, 2008) migrate slowly from the SVZ towards the cortical plate (CP) (Britanova *et al*, 2008). They begin entering the CP at E18.5 in the mouse and complete their migration by P2 (Tarabykin *et al*, 2001). Instead, neurons that express the marker Satb2, although born simultaneously or even later than Unc5D+ neurons, do not linger in the SVZ and arrive in the CP as early as E14.5. The molecular mechanisms underlying this different migratory behaviour are not understood. The functional significance of Unc5D expression in BPs is currently unclear, but it raises the possibility that Unc5D is involved in controlling or modulating radial migration towards the CP. Since FLRT2 is expressed in the developing neocortex, we investigated the possibility that FLRT2/Unc5D signalling provides guidance to migrating cells and/or pathfinding axons.

Here, we show that all three FLRT ECDs undergo cleavage by metalloproteases and are shed from cultured neurons, suggesting non-cell autonomous functions. Our results revealed specific and high-affinity interactions between FLRT2 and Unc5D (and to a lesser extent Unc5B) and between FLRT3 and Unc5B receptors. Further, we found that soluble FLRT ECDs activate Unc5 repulsive signalling inducing growth cone collapse and cell sorting. *In vivo*, Unc5D and FLRT2 modulate the radial migration of cortical cells. During corticogenesis, FLRT2 is expressed in cells of the CP at the time when Unc5D+ cells in the SVZ display their delayed migratory behaviour. Using a combination of gain- and loss-of-function experiments in the mouse, we show that FLRT2 and Unc5D have a significant impact on the migration of a subset of projection neurons, consistent with FLRT2 acting as a repulsive cue for Unc5D+ cells.

Results

The ECDs of FLRTs are shed from neurons

To investigate posttranslational modifications of FLRT proteins, we transfected HEK293T cells with epitope-tagged constructs and examined the proteins in cell lysates and culture media by western blotting. In cell lysates, antibodies against the individual FLRT1–3 ECDs specifically detected full-length FLRT proteins and showed no crossreactivity with the other FLRTs (Figure 1A). Interestingly, all three FLRT ECDs were detected in conditioned media of the cultures after pull down with a lectin that recognizes glycoproteins (Figure 1A). The sizes of the cleaved ECDs ranged from 65 to 85 kDa, suggesting a cleavage event near the plasma membrane. Whereas FLRT1 and FLRT3 ECDs consisted of a single protein species, the FLRT2 ECD was a doublet of 75 and 85 kDa (Figure 1A). The analysis of total cell lysates from transfected cells confirmed the presence of low molecular weight bands containing the C-terminal FLAG tag (Figure 1B). Cleavage of the FLRT2 ECD was also detected with a FLRT2 deletion mutant lacking the entire intracellular domain (ICD), indicating that the ICD was not required for FLRT2 ECD shedding (Figure 1C). Endogenous FLRT ECDs were also shed from primary mouse neurons (glial cells express low levels of FLRT2; Supplementary Figure S1). We detected FLRT1–3 ECD species in conditioned media of dissociated embryonic cortical neurons and the ECD sizes matched those of transfected FLRTs, including the doublet of the FLRT2 ECD (Figure 1D, top panels). The proteins in the media were not detected by antibodies against the ICD of FLRTs (Figure 1D, lower panels). The amount of shed FLRT2 ECD in the media of hippocampal neurons remained stable for up to 10 DIV, while the full-length expression in the neurons decreased (Figure 1C). The FLRT2 ECD was even detectable in conditioned media from hippocampal explants of subregion CA1 (Figure 1E) where FLRT2 was strongly expressed (Figure 7A). The specificity of the signal in the culture media was confirmed by using the corresponding cells from *FLRT2*$^{-/-}$ and *Nestin-Cre*$^{+}$*;FLRT3*$^{lx/-}$ mice (Figure 1E and F; Supplementary Figure S1). We then performed immunoblots of developing brain extracts and detected FLRT1 proteins from E13 to P10 at similar levels, while FLRT2 and FLRT3 expression gradually decreased after E15 (Figure 2A–C). Anti-FLRT ECD antibodies detected a 90-kDa species and an additional band in the range of 65–70 kDa in the cases of FLRT1 and FLRT3, or a doublet of 73 and 80 kDa in the case of FLRT2 (Figure 2A–C, upper panels), whereas anti-FLRT ICD antibodies detected only a single protein species of ~90 kDa (Figure 2A–C, lower panels). None of these proteins were detected in the corresponding knockout brain extracts (Figure 2A–C). Since the entire polypeptide of each of the FLRTs is encoded by a single exon (Lacy *et al*, 1999), these different protein species could not have resulted from alternative splicing. In addition, glycosidase treatment of brain extracts converted all protein species (full-length and ECDs) to faster migrating ones to similar extents, indicating that the additional bands detected by the anti-FLRT ECD antibodies were not hypoglycosylated forms, but rather proteolytic cleavage products of the mature FLRTs (Figure 2D–F).

To test whether metalloproteases were involved in FLRT ECD shedding, we examined FLRT2 and FLRT3 expression in the presence of the wide spectrum matrix metalloproteinases and ADAM inhibitors TAPI-0, TAPI-I and GM6001 (Budagian *et al*, 2005). All three inhibitors markedly reduced the release of the FLRT3 ECD into the conditioned media of cultured neurons (Figure 2G and H). TAPI-I, when analysed for its involvement in FLRT2 cleavage, also reduced the release of the FLRT2 ECD, although somewhat higher concentrations were required (Figure 2I). In contrast, DAPT, an inhibitor of the γ-secretase protease complex (Geling *et al*, 2002) did not affect FLRT2/3 ECD shedding (data not shown). These results suggest that FLRT ECD shedding is an active process that requires metalloprotease activity.

To begin mapping the site of FLRT ECD cleavage, we generated different isoforms of FLRT2 and FLRT3 carrying small deletions in the ECD (Figure 2J and L). Expression controls of these constructs by immunofluorescence and in total cell lysates showed that they were expressed at similar levels in the membrane of transfected HEK293T cells (Figure 2K and M; Supplementary Figure S2). Whereas the deletion of the FNIII domain did not change the abundance of the FLRT3 ECD in the conditioned media, the deletion of the juxtamembrane (JM) region completely blocked release of

the FLRT3 ECD (Figure 2K). The two cleavage sites of FLRT2 were also mapped to the JM region and flanking a conserved *N*-glycosylation site, which is required for proper expression in the cell membrane (Figure 2M and data not shown).

Soluble FLRT ECDs bind to Unc5 receptors

To identify interaction partners for FLRT ECDs, we used soluble FLRT ECDs fused to alkaline phosphatase (AP) as baits in binding assays on transfected HEK293T cells expres-

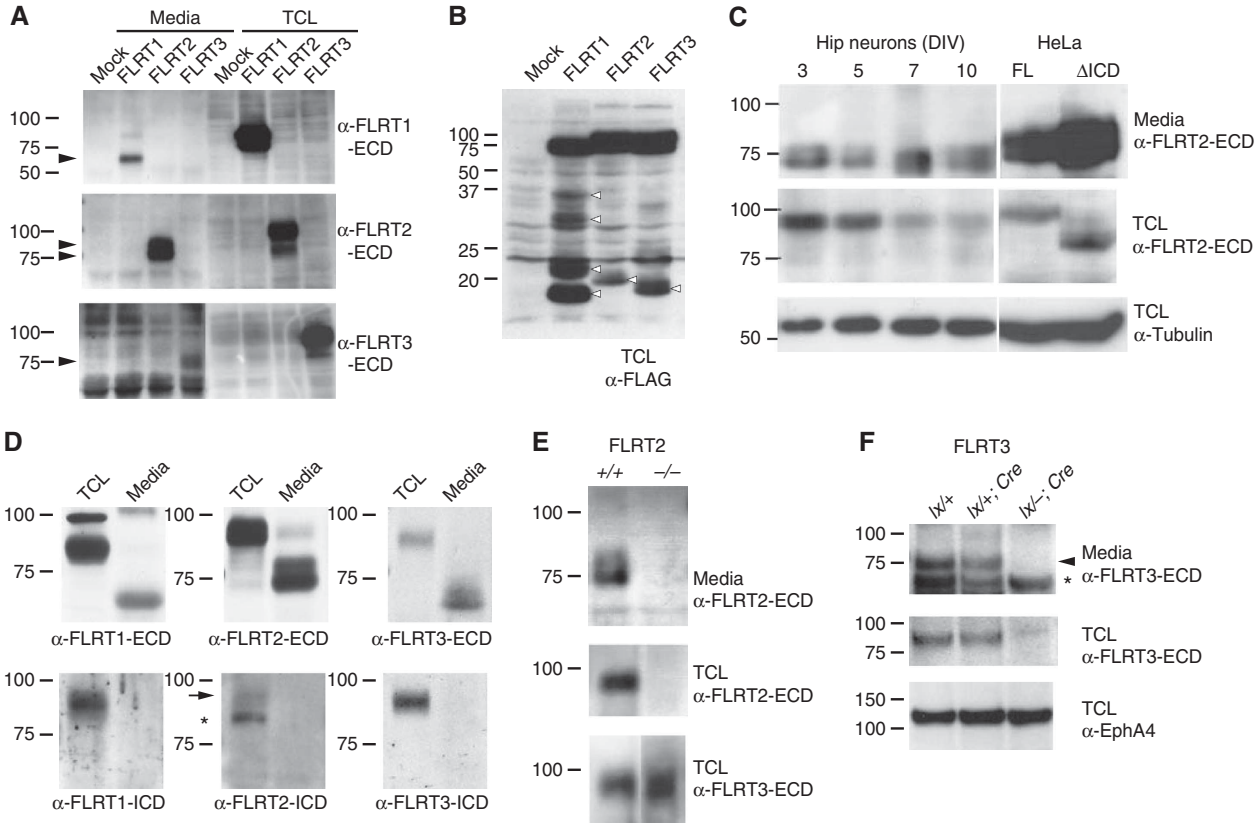

Figure 1 FLRT ECDs are shed from transfected cells and neurons. (**A**, **B**) Western blot analysis of lectin pull-down (glycoprotein enriched) samples from 2 DIV conditioned media (Media) or of corresponding total cell lysates (TCL in **A**, **B**) of HEK293T cells transfected with C-terminally FLAG-tagged FLRT1, FLRT2, FLRT3 or Mock transfected. Samples were analysed using antibodies against the ECD of FLRTs or FLAG as indicated. Arrowheads in (**A**) point to the FLRT ECDs (one species for FLRT1 or FLRT3, doublet for FLRT2). Various protein species in the range of 18–35 kDa were found in the TCL (arrowheads in **B**). (**C**) Same analysis as in (**A**) of dissociated E17.5 hippocampal neurons kept in culture for the indicated DIV or HeLa cells transiently transfected with C-terminally FLAG-tagged full-length FLRT2 (FL) and FLRT2 lacking the intracellular domain (ΔICD). Anti-tubulin levels in TCLs are shown as loading controls. (**D**) Detection of shed FLRT1–3 ECDs in 6 DIV conditioned media of E16.5 cortical neurons. FLRT1–3 ECDs are visible in blots probed with anti-ECD antibodies (upper panels) but not with anti-ICD antibodies (lower panels). The positions of full-length FLRT2 (arrow) and of a non-specific band (asterisk) are indicated (see FLRT2$^{-/-}$ control in Figure 2B). (**E**, **F**) Mouse mutants demonstrate specificity of the ECD signals. (Upper panels) Western blot analysis of glycoprotein enriched samples of 7 DIV conditioned media from CA1 hippocampal explants (**E**) or dissociated cortical neurons (**F**) of the indicated genotypes using anti-FLRT2/3 ECD antibodies. (Middle panels) Corresponding glycoprotein enriched TCL probed with anti-FLRT2/3 ECD antibodies. (Lower panel) Corresponding glycoprotein enriched TCL probed with a loading control (anti-FLRT3 ECD in (**E**) and anti-EphA4 in (**F**)). Arrowhead and asterisk in (**F**) indicate FLRT ECD and a non-specific band, respectively (see also Supplementary Figure S1).

Figure 2 Cleaved FLRT ECDs in developing brain and involvement of metalloproteases. (**A**–**C**) Cleaved FLRT ECDs in brain extracts. Western blot analysis of glycoprotein enriched brain extracts of the indicated developmental stages using antibodies against the FLRT ECDs (upper panels) or FLRT-ICD (lower panels) (first lanes contain extracts from the indicated knockout animals). Arrowheads indicate the positions of the FLRT ECDs. The positions of full-length FLRTs (arrow) are indicated. (**D**–**F**) FLRT ECDs are glycosylated. Glycoprotein enriched E13 brain extracts followed by incubation with (+) or without (−) *N*-glycosidase were analysed as above. Arrows and arrowheads indicate full-length and shed FLRT proteins, respectively. (**G**–**I**) Involvement of metalloproteases in FLRT shedding. Dissociated E16.5 cortical neurons were cultured for 2 DIV plus one additional DIV in the presence of 10 μM of TAPI-0, 10 μM (or 50 μM) of TAPI-I and 5 μM of GM6001 or vehicle only (DMSO). Glycoprotein enriched samples from the media and the total cell lysates (TCL) were analysed by western blotting using anti-FLRT ECD antibodies. Arrowheads in panels (**G**, **H**) indicate the position of the FLRT3 ECD. Asterisk in (**G**) indicates the position of a non-specific band (see also (**K**) and Figure 1F). (**J**–**M**) Mapping the cleavage site in FLRT3 and FLRT2 ECDs. (**J**, **L**) Scheme of deletion mutants used (all C-terminal FLAG-tagged; FLRT2 constructs also had an N-terminal Myc tag). (**J**) ΔFNIII lacking the fibronectin type III domain (amino acids 406–501) and ΔJM lacking the JM region (amino acids 502–523) of FLRT3. (**L**) ΔJM1 lacking amino acids 512–520, ΔJM2 lacking amino acids 524–536 and ΔJM1 + 2 lacking amino acids 512–536 but keeping the NGS sequence of the *N*-glycosylation site of the JM region of FLRT2. (**K**, **M**) Western blot analysis of glycoprotein enriched media of HEK293T cells transfected with the above constructs or EGFP (GFP). Samples were analysed using antibodies against FLRT3 ECD (**K**) or Myc (**L**, **M**) (upper panels). Expression in total cell lysates (TCL) was analysed using an anti-FLAG antibody (lower panels). Arrowheads indicate the position of the cleaved ECDs and asterisk in (**K**) indicate the position of a non-specific band (see also Supplementary Figure S2 for protein expression in plasma membrane).

sing candidate interaction partners. Although FLRT3 promoted homotypic cell aggregation (Karaulanov *et al*, 2006; Egea *et al*, 2008), we found that FLRT3/ECD-AP did not bind any of the three FLRT proteins (Supplementary Figure S3). Moreover, FLRT2 ECD equally bound to cultured *FLRT2*$^{-/-}$ neurons compared with wild-type controls (Supplementary Figure S3), arguing against FLRT proteins interacting with other FLRTs. FLRT3 binding to the Wnt receptor Brother of

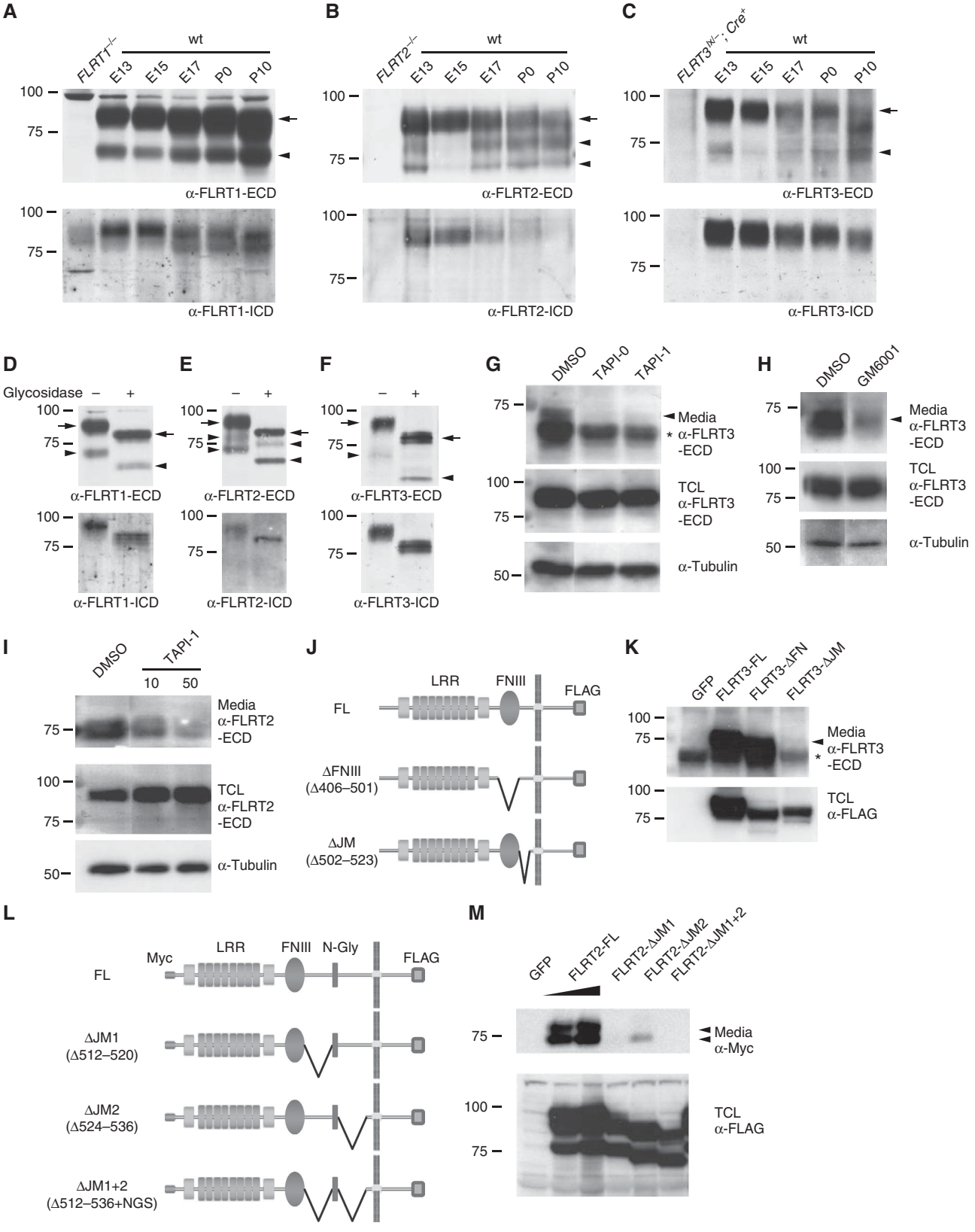

CDO (BOC), as recently shown for *Zebrafish* FLRT3 (Sollner and Wright, 2009), could not be confirmed for mouse FLRT3, nor did we detect specific binding to FGFR2 or the Netrin receptor Neogenin (Supplementary Figure S3). In agreement with published reports (Karaulanov *et al*, 2009; Sollner and Wright, 2009), FLRT3/ECD-AP strongly bound to cells transfected with the Netrin receptor Unc5B (Figure 3B and G; Supplementary Figure S3). A comparison between all three FLRTs and the entire Unc5 protein family (Unc5A–D) revealed that Unc5B was the preferred binding partner for FLRT3, with an equilibrium dissociation constant (Kd) of 66 nM ($n=5$ experiments; Figure 3B, D, K and L; Supplementary Figure S3). Interestingly, FLRT2 displayed a different binding pattern with strong affinity for Unc5D (Kd of 11 nM, $n=4$; Figure 3C, G, I and J; Supplementary Figure S3) and weaker binding to Unc5B (Figure 3A, G and I). A naturally occurring splice variant of Unc5D lacking the first thrombospondin-1 domain (Unc5DΔTP1, accession number BC145695), which is predicted to still bind to Netrin (Kruger *et al*, 2004), failed to bind to FLRT2 (Figure 3E,G). FLRT1 showed only relatively weak binding to Unc5B and none of the FLRTs displayed strong interaction with Unc5A or Unc5C (data not shown). We confirmed the specificity of FLRT–Unc5 interactions by reciprocal binding experiments: HEK293T cells were transfected with full-length FLAG-tagged FLRTs and incubated with soluble Unc5B/ECD-Fc, Unc5D/ECD-Fc or Fc as control. The Unc5D/ECD showed the strongest preference for FLRT2, while Unc5B/ECD preferred FLRT3 over FLRT2 (Figure 3M–T). The interaction between FLRTs and Unc5 proteins appeared to be independent of Netrin-1. Netrin-1 did not bind FLRT2 in the absence of Unc5D and rather competed with FLRT2-AP for binding to Unc5D (Supplementary Figure S3).

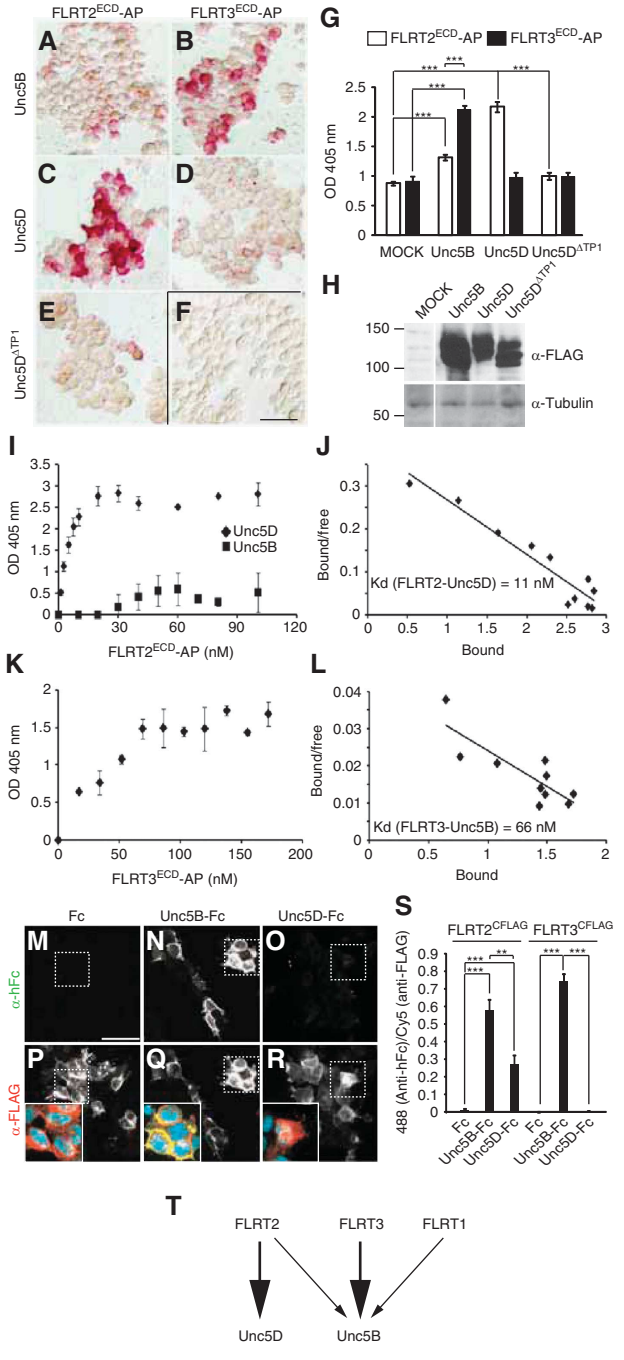

Figure 3 Soluble FLRT ECDs bind to Unc5 receptors. (**A**–**H**) FLRT2 binds best to Unc5D and to a lesser extent to Unc5B, while FLRT3 shows strong preference to Unc5B. Transfected HEK293T cells (MOCK empty vector or C-terminally FLAG-tagged Unc5B, Unc5D or Unc5D$^{\Delta TP1}$ were incubated with similar amounts (250 nM) of FLRT2/ECD-AP or FLRT3/ECD-AP fusion proteins, as indicated. AP activity was revealed using Naphtol-Fast Red (**A**–**F**) or by absorbance at 405 nm using *p*-nitrophenylphosphate (**G**). (**G**) Representative plot of average activity + s.e.m ($n=3$) ($P<0.001$, *t*-test). Expression of the transfected constructs was analysed by western blot using an anti-FLAG antibody (**H**) (lanes belong to the same gel and western blot). Tubulin was used as loading control. Scale bar in (**F**): 50 μm. (**I**–**L**) Dose–response curves (**I**, **K**) of the binding affinity of FLRT2/ECD-AP towards Unc5D or Unc5B and FLRT3/ECD-AP towards Unc5B in transiently transfected HEK293T cells. (**J**, **L**) Scatchard plots and average binding affinity ($n>3$ independent experiments) of the FLRT2/ECD-Unc5D (**J**) and FLRT3/ECD-Unc5B (**L**) interactions. (**M**–**S**) Soluble Unc5B/ECD-Fc, but not Unc5D/ECD-Fc, binds HEK293T cells transfected with C-terminally FLAG-tagged FLRT3. Cells were incubated as indicated with control Fc, Unc5B/ECD-Fc or Unc5D/ECD-Fc, fixed and stained by immunofluorescence with anti-hFc (bound protein; green channel in insets in lower row) and anti-FLAG (transfected protein; red channel in insets in lower row). Co-localization is shown in yellow in the overlay (**Q**, inset). (**S**) Results of a representative experiment (average + s.e.m., $n=2$) of the bound fractions of Unc5D/ECD-Fc, Unc5B/ECD-Fc and Fc normalized to the amount of transfected FLRT ($^{**}P<0.01$; $^{***}P<0.001$, *t*-test). Scale bar in (**M**): 50 μm. (**T**) Summary of the binding affinities of FLRTs to Unc5 receptors (see also Supplementary Figure S3).

Soluble FLRT2/3 ECDs induce growth cone collapse of cortical neurons via Unc5 receptors

Next, we used dissociated neuron cultures of E16.5 rat motor cortices, which endogenously express Unc5B and Unc5D (see mouse expression data in Supplementary Figure S6 and Figure 7B), to assess whether FLRT/ECD binding to Unc5 receptors would be sufficient to activate their repulsive signalling properties. We counted the number of collapsed growth cones after staining with phalloidin to visualize the actin cytoskeleton. All phalloidin-stained neurons were included in the analysis, although only ~50% of them specifically bound FLRT3-Fc (Figure 4A–C). Stimulation with different concentrations of FLRT3-Fc-induced growth cone collapse

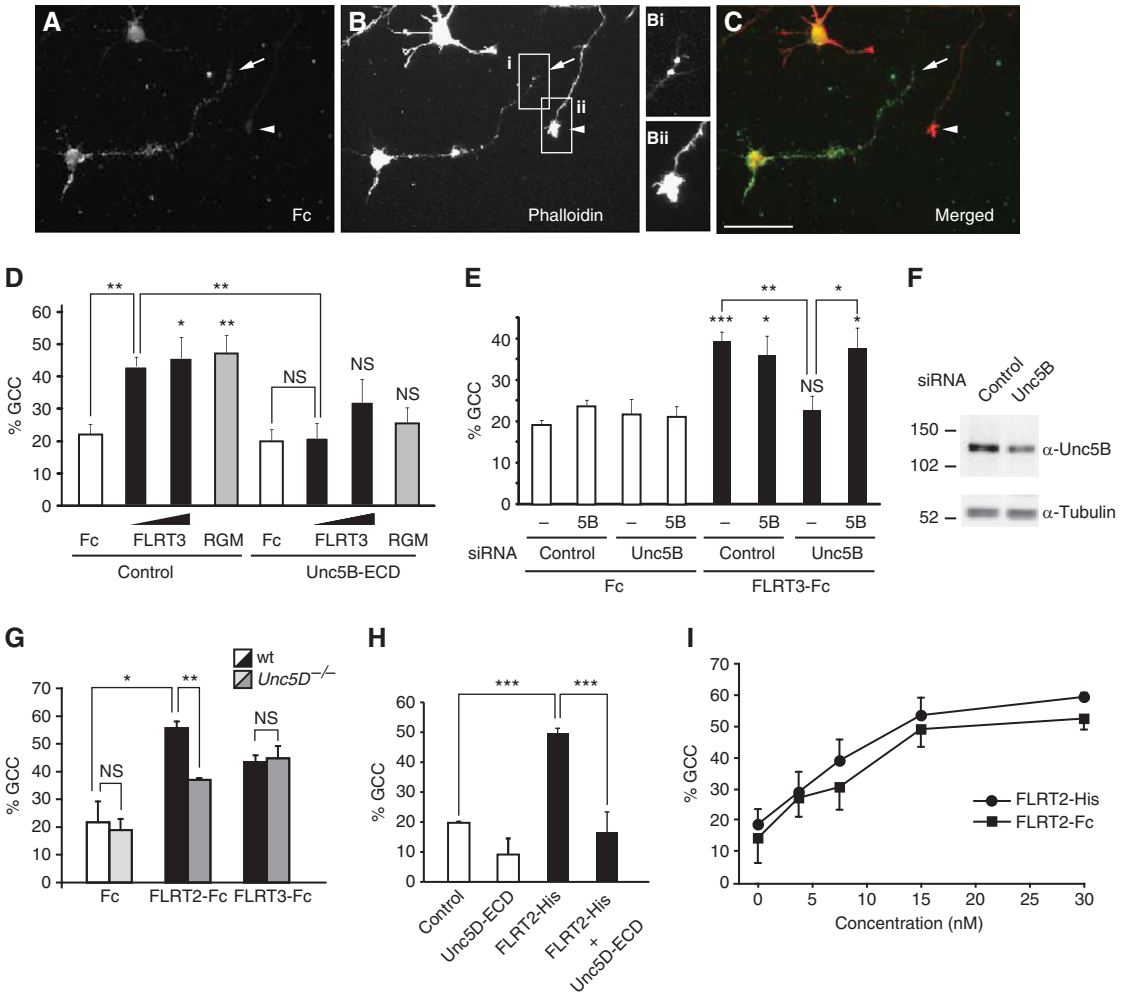

Figure 4 FLRT2/3 ECDs induce growth cone collapse of cortical neurons via Unc5. (**A**–**C**) Representative examples of phalloidin-stained rat embryonic cortical neurons stimulated with 1 μg/ml FLRT3-Fc. Anti-Fc antibody staining shows a neuron with a collapsed, phalloidin-negative growth cone (arrow in **B**, **Bi**). Two other neurons (in one case only the axon is visible) do not show FLRT3-Fc binding and have intact growth cones (arrowhead in **B**, **Bii**). Scale bar: 50 μm. (**D**) The soluble Unc5B ectodomain (Unc5B-ECD) inhibits growth cone collapse of rat cortical neurons (expressing endogenous Unc5B) induced by FLRT3-Fc (1 and 3 μg/ml) and RGMa (2 μg/ml). The average (+s.e.m.) is shown (three independent experiments). (**E**, **F**) Knockdown of endogenous Unc5B by specific siRNA abolishes FLRT3-Fc-induced growth cone collapse. Rat cortical neurons were transfected with control or Unc5B siRNA in the presence or absence of mock or Unc5B expression vector. (**F**) Western blot against Unc5B showing the efficiency of the RNAi in (**E**) (>60% reduction, upper panel). Tubulin was used as loading control (lower panel). (**G**) *Unc5D*$^{-/-}$ cortical neurons display reduced collapse response to 3 μg/ml FLRT2-Fc. E15.5 neurons from the motor cortex of wild-type or *Unc5D*$^{-/-}$ mice were treated as described in (**A**–**E**). The graph shows the average (+s.e.m.) of two independent experiments (3–6 coverslips per condition, >20 neurons per coverslip). (**H**) FLRT2 carrying a small, non-dimerizing His tag (FLRT2-His; 3 μg/ml–37.5 nM) is also active in promoting growth cone collapse in E16.5 mouse cortical neuron cultures as FLRT2-Fc. The effects of FLRT2-His were abolished after preincubation with 5 μg/ml Unc5D-Fc (50 nM). (**I**) Dose–response curves of growth cone collapse induced by FLRT2-His or FLRT2-Fc. in E16.5 mouse cortical neurons. The differences are not significant. (NS, not significant; *$P<0.05$, **$P<0.01$, ***$P<0.001$, *t*-test).

comparable to RGMa, a ligand for Unc5B/Neogenin complex (Figure 4D; Hata *et al*, 2009). Both responses were significantly reduced in the presence of the soluble Unc5B/ECD, which presumably blocked the active sites of FLRT3-Fc or RGM (Figure 4D). We next performed growth cone collapse assays on cortical neurons in which the endogenous Unc5B expression was reduced by siRNA-mediated knockdown and observed that the FLRT3-Fc-induced collapse response was completely abolished (Figure 4E and F). This effect was specific since overexpression of Unc5B together with the siRNA-mediated knockdown, restored the collapse response induced by FLRT3-Fc (Figure 4E). Next, we turned to FLRT2 and its Unc5D receptor and generated *Unc5D*$^{-/-}$ mice (Supplementary Figure S4). *Unc5D*$^{-/-}$ mice were viable and did not display obvious behavioural defects. Gross inspection of forebrain anatomy did not reveal major anatomical defects (data not shown). The growth cone collapse response of *Unc5D*$^{-/-}$ cortical neurons towards FLRT2-Fc, but not FLRT3-Fc, was significantly impaired compared with cultures derived from wild-type littermates, indicating the specific binding to FLRT2 (Figure 4G). Finally, a similar dose- and Unc5D-dependent collapse response was observed using a FLRT2 ECD carrying a small, non-dimerizing epitope tag (FLRT2-His) (Figure 4H and I), providing support for the concept that the native shed FLRT2 ECD is active. Together, these results provide strong evidence that FLRT2/3 ECDs act as repulsive cues for cortical axons *in vitro* through a mechanism that requires Unc5 receptors.

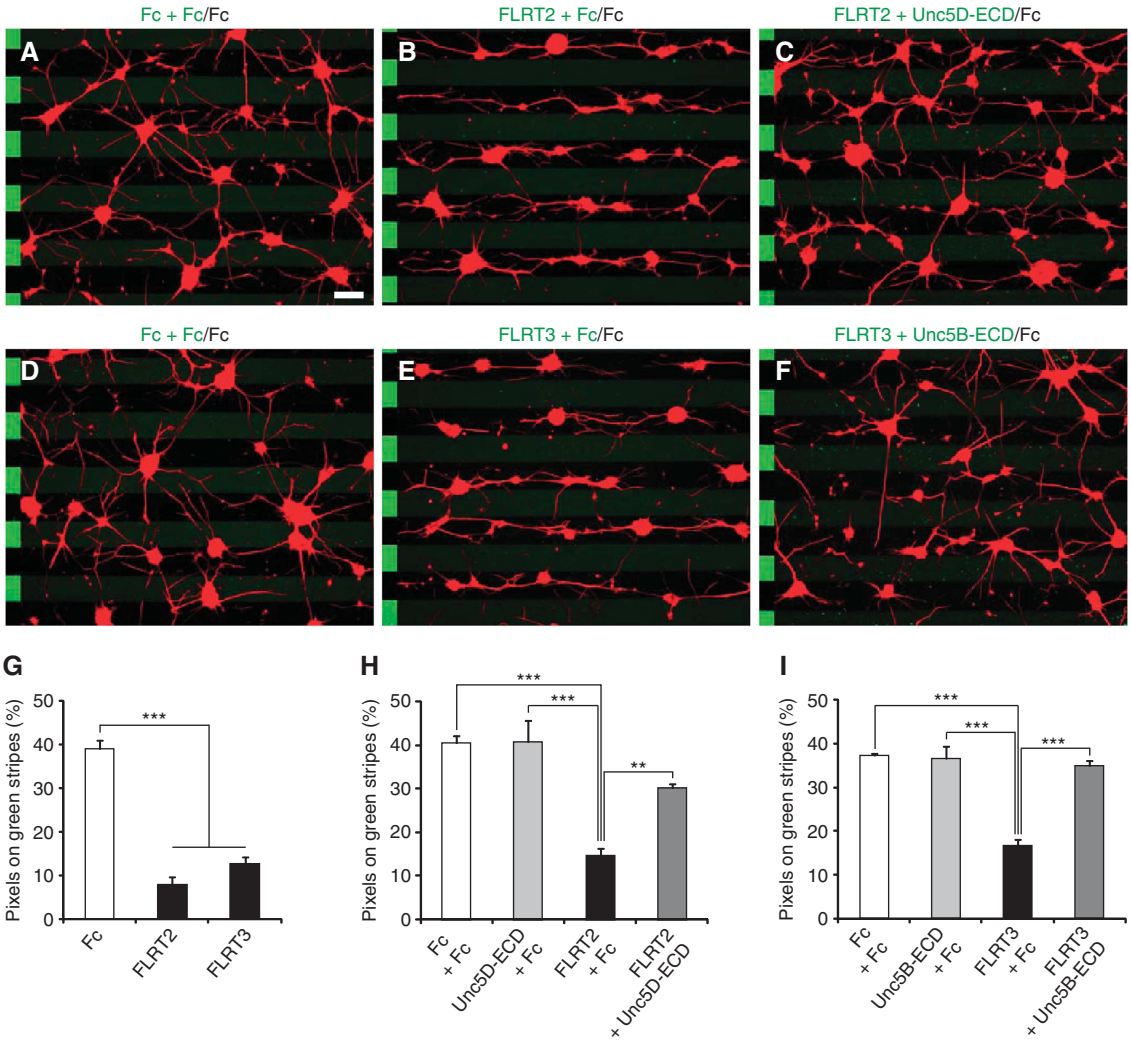

Figure 5 Stripe assays with FLRT2/3 ECDs and hippocampal neurons. (**A**–**F**) E15.5 hippocampal neurons were grown on stripes containing (**A**, **D**) control Fc preincubated with control Fc (green) against control Fc (black), (**B**) FLRT2-Fc and (**E**) FLRT3-Fc preincubated with control Fc (green) against control Fc (black), (**C**) FLRT2-Fc preincubated with Unc5D-ECD-Fc (green) against control Fc (black), (**F**) FLRT3-Fc preincubated with Unc5B-ECD-Fc (green) against control Fc (black). Cells were stained with anti-Tau1 antibodies to visualize axons (red). The location of the faintly stained green stripes is indicated by alternating stripes on the left side of each image. FLRT2/3-Fc had repulsive effects on both axons and soma (see Supplementary Figure S5). Scale bar: 100 μm. (**G**–**I**) Images were digitalized and the percentage of Tau1 + pixels on green stripes was quantified. (**G**) Maximal repulsion by FLRT2-Fc and FLRT3-Fc without dilution with control Fc. (**H**, **I**) Inhibition of FLRT2/3-induced repulsion by preincubation with the respective Unc5-ECD-Fc proteins ($n = 3$ independent experiments, $^{**}P < 0.01$, $^{***}P < 0.001$, *t*-test).

FLRT2/3-Fc proteins repel axons and soma of hippocampal neurons

Next, we used the stripe assay (Vielmetter *et al*, 1990), to test whether neurons would show a growth preference when given a choice between FLRT+ and FLRT− stripes. For this, we used hippocampal or cortical neurons since they expressed Unc5B and Unc5D (Supplementary Figure S6). We arranged carpets of stripes of purified FLRT2-Fc or FLRT3-Fc, alternating with control Fc, and grew dissociated E15.5 neurons on these stripes for 1 day. Neurons were either imaged with time-lapse video microscopy or fixed and stained with the axon-specific marker Tau1. Hippocampal neurons were strongly repelled from the FLRT2-Fc and FLRT3-Fc stripes; thus, they preferentially grew on the control stripes (Figure 5A, B, D, E and G; Supplementary Figure S5 and Movies S1 and S2). Similar effects were observed for FLRT2-Fc in cortical neurons (Supplementary Figure S5). When calculating the proportion of Tau+ pixels on FLRT-Fc-containing stripes, only 8–13% were found on FLRT2-Fc and FLRT3-Fc stripes, respectively (Figure 5G), while on Fc versus Fc stripes Tau1+ pixels were distributed in nearly random manner. When the distributions of axons and soma were calculated separately, we found that both were equally sensitive to the repulsive effects of FLRT2/3-Fc (Supplementary Figure S5). When FLRT2/3-Fc proteins were preincubated with the respective Unc5-ECDs, they no longer had repulsive activity in the stripe assay, suggesting that this function depended on the specific interaction with Unc5 receptors (Figure 5C, F, H and I).

We also found that this effect was not due to differential adhesion to the FLRT-containing stripes, since at early time points after plating (2 h), there were no significant differences in the percentages of cells on Fc versus FLRT stripes (Figure 6A–C). At 4 h after plating, however, the numbers of cells on

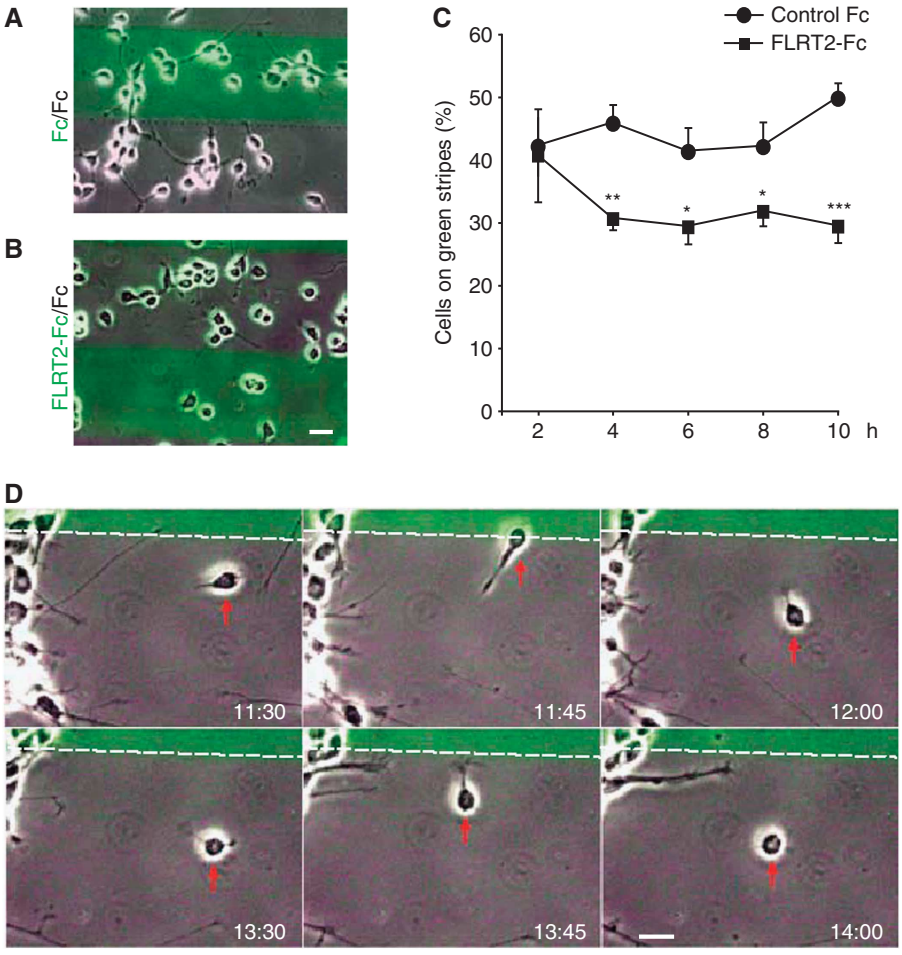

Figure 6 FLRT2 ECD has repulsive effects on cultured neurons. (**A**–**C**) Dissociated hippocampal neurons from E15.5 brains were plated on stripes containing control Fc versus control Fc (**A**), or FLRT2-Fc versus control Fc (**B**) and imaged every 2 h. The images in (**A**, **B**) shown at 4 h time point. (**C**) At the indicated time points after plating, neurons in each stripe were counted and the percentage of cells on the green stripes (%) plotted as indicated as the mean value + s.e.m. (five independent fields from two experiments with >70 to 140 neurons were counted per field and condition; $*P<0.05$, $**P<0.01$, $***P<0.001$, *t*-test). (**D**) Frames at the indicated time points (h:m) after plating of a representative movie showing the dynamics of hippocampal neurons (E15.5) on the stripes. The cell marked by a red arrow is repelled twice from the stripe containing the FLRT2-Fc protein. The boundary between stripes is indicated with a stippled line and the FLRT2-Fc protein is located in the upper, green stripe. The original movie can be accessed from Supplementary Movie S1. Scale bar: 20 μm.

the FLRT2-Fc stripes had significantly decreased and this segregation continued for the entire time of analysis (up to 10h; Figure 6C). Time-lapse imaging revealed that single neurons displayed a rather dynamic behaviour on the stripes and upon contact actively moved away from FLRT2-Fc stripes (Figure 6D). Taken together, these observations indicate that FLRT ECD proteins repel cell bodies and their axons.

FLRT2 and Unc5D expression in cerebral cortex

FLRT2 and Unc5D were strongly expressed in the neocortex, hippocampus and other brain areas of the developing brain (Figure 7A and B). Interestingly, the *in situ* hybridization (ISH) pattern of FLRT2 expression in the neocortex did not exactly overlap with the FLRT2 protein distribution. At E15.5, FLRT2 mRNA was confined to the CP, whereas FLRT2 immunoreactivity was detected in the CP and more apical regions such as intermediate zone (IZ) and SVZs (Figure 7C–E). This was confirmed by microdissection experiments where the marginal zone (MZ) and CP were mechanically separated from the SVZ + VZ. In these experiments, we observed a significant enrichment of the FLRT2 ECD compared with the full-length protein, consistent with the model that the FLRT2 ECD is cleaved and shed from FLRT2-expressing cells *in vivo* (Figure 7F and G).

At E15.5, multipolar cells expressing Unc5D or svet1, which comprises a non-coding RNA encoded by an intronic region of the unspliced RNA of Unc5D, were located in the SVZ (Figure 7I and J) (Sasaki *et al*, 2008), well separated from FLRT2-expressing cells (Figure 7H), but in reach for the shed FLRT2 ECD (Figure 7D). Later in development, FLRT2 and Unc5D/Svet1 patterns changed, but were always non-overlapping (Figure 7K–P). At E17.5–18.5, FLRT2 continued to be expressed in cortical layers. In contrast, the bulk of svet1-positive cells were found in SVZ. Scattered svet1-positive cells were spread throughout the cortex and the svet1 signal always appeared condensed in a single spot (probably nuclear (Sasaki *et al*, 2008); Figure 7M and M′). The bulk of Unc5D-positive cells were also found in the SVZ, but the Unc5D signal in CP and IZ was very weak (Figure 7L). The few migratory cells detected with the Unc5D ISH probe showed a condensed signal similar to svet1, suggesting that

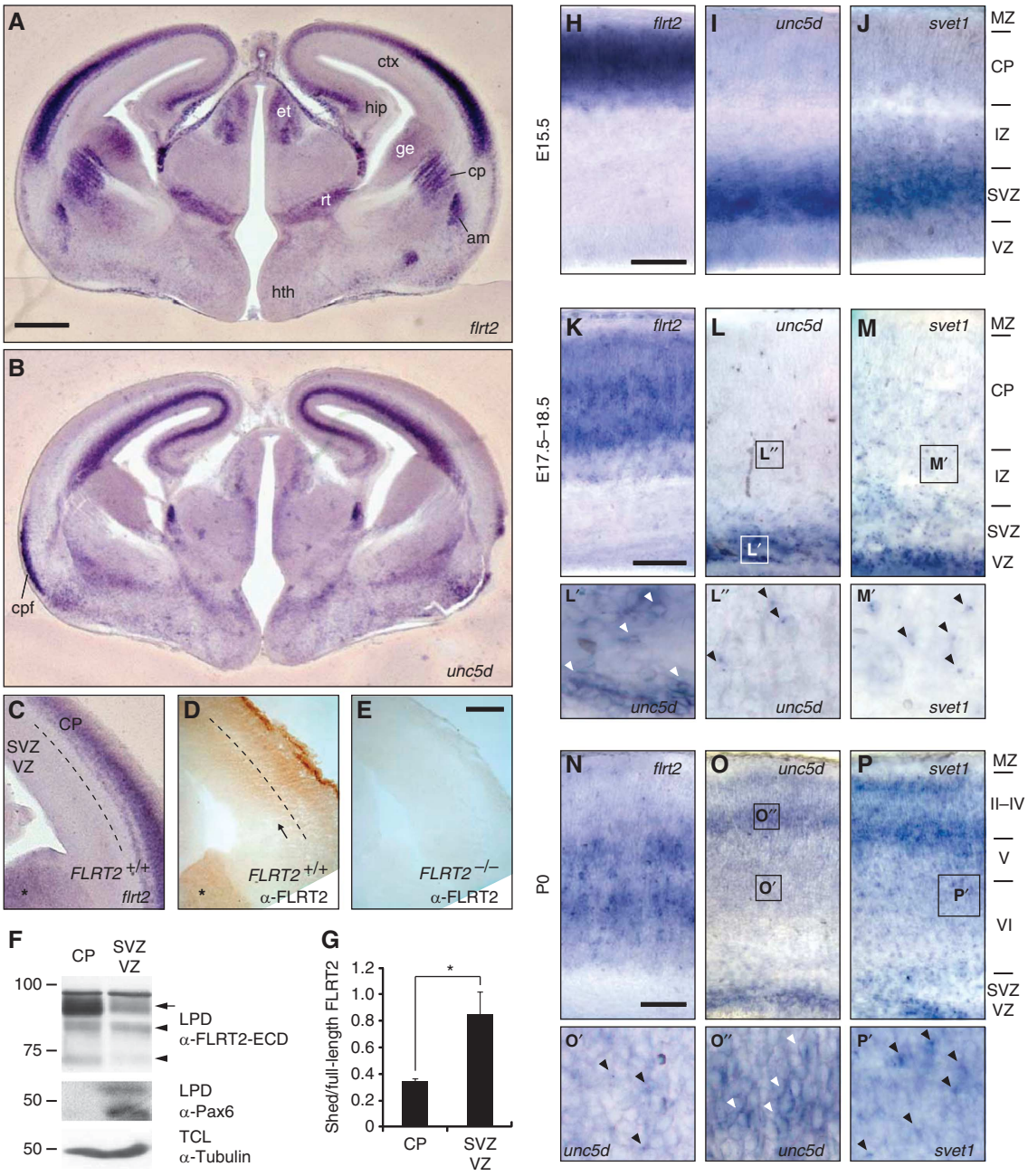

Figure 7 FLRT2 and Unc5D expression in cerebral cortex and Unc5D downregulation during migration. (**A**–**C**, **H**–**P**) ISH analyses and immunohistochemistry (IHC) (**D**, **E**) of coronal brain sections at E15.5 (**A**–**E**, **H**–**J**), E17.5 (**K**), E18.5 (**L**, **M**) and P0 (**N**–**P**) using the indicated digoxigenin-labelled antisense probes. Overview pictures of the whole brain (**A**, **B**) or details of the dorsal neocortex (**C**–**E**, **H**–**P**). FLRT2 expression does not overlap with that of Unc5D/svet1 in most brain regions (**A**, **B**, **H**–**J**). IHC with antibodies raised against the extracellular domain of FLRT2 give positive signals in the SVZ area of E15.5 cortex below the region labelled with the FLRT2 ISH probe (**D**, arrow). Asterisks in (**C**, **D**) indicate the ganglionic eminence. FLRT2 immunoreactivity is absent in FLRT2 KO sections (**E**). (**F**, **G**) Microdissection of the CP (+MZ) and the SVZ + VZ regions from slices of E15.5 cortex. Dashed line in (**C**, **D**) indicates the region (around the IZ) where the dissection was made. (**F**) Protein lysates of the dissected tissues were subjected to lectin pull down (LPD) and samples were blotted with antibodies against FLRT2 ECD (upper panel) and the VZ marker Pax6 (middle panel) (Walther and Gruss, 1991; Lefebvre *et al*, 2002). Tubulin in the total cell lysates (TCL) was used as loading control (lower panel). Arrow and arrowheads point to the full-length and shed species of FLRT2, respectively. (**G**) Quantification of the relative amount of shed FLRT2 ECD species compared with full-length ($n = 3$ independent microdissections, $^*P < 0.05$; *t*-test). (**H**–**P**) Unc5D and svet1 patterns are nearly identical in the neocortex of all the developmental stages analysed. The notable exceptions are IZ and CP at 18.5: Unc5D expression is very low, whereas svet1 labels scattered cells (**L**, **M**). At P0, the topography of FLRT2/Unc5D/svet1 expression has reversed compared with earlier stages (**N**–**P**). Stationary cells show a cytoplasmic expression pattern (**L′**, **O″**, white arrowheads), migratory cells show a condensed, possibly nuclear signal (**L″**, **M′**, **O′**, **P′**, black arrowheads). am, amygdala; cp, caudate putamen; cpf, pyriform cortex; ctx, cortex; et, epithalamus; ge, ganglionic eminence; hip, hippocampus; hth, hypothalamus; rt, thalamic reticular nucleus. Scale bars: (**A**, **B**) 500 μm; (**E**, **H**, **K**, **N**) 100 μm (see also Supplementary Figure S6).

the predominant Unc5D RNA was unspliced and that the spliced Unc5D mRNA was specifically downregulated (Figure 7L″). This was in contrast to the more cytoplasmic pattern of Unc5D expression in the SVZ (Figure 7L′). At P0, the topography of FLRT2/Unc5D/svet1 expression had reversed (Figure 7N–P): Unc5D/svet1 expression was now

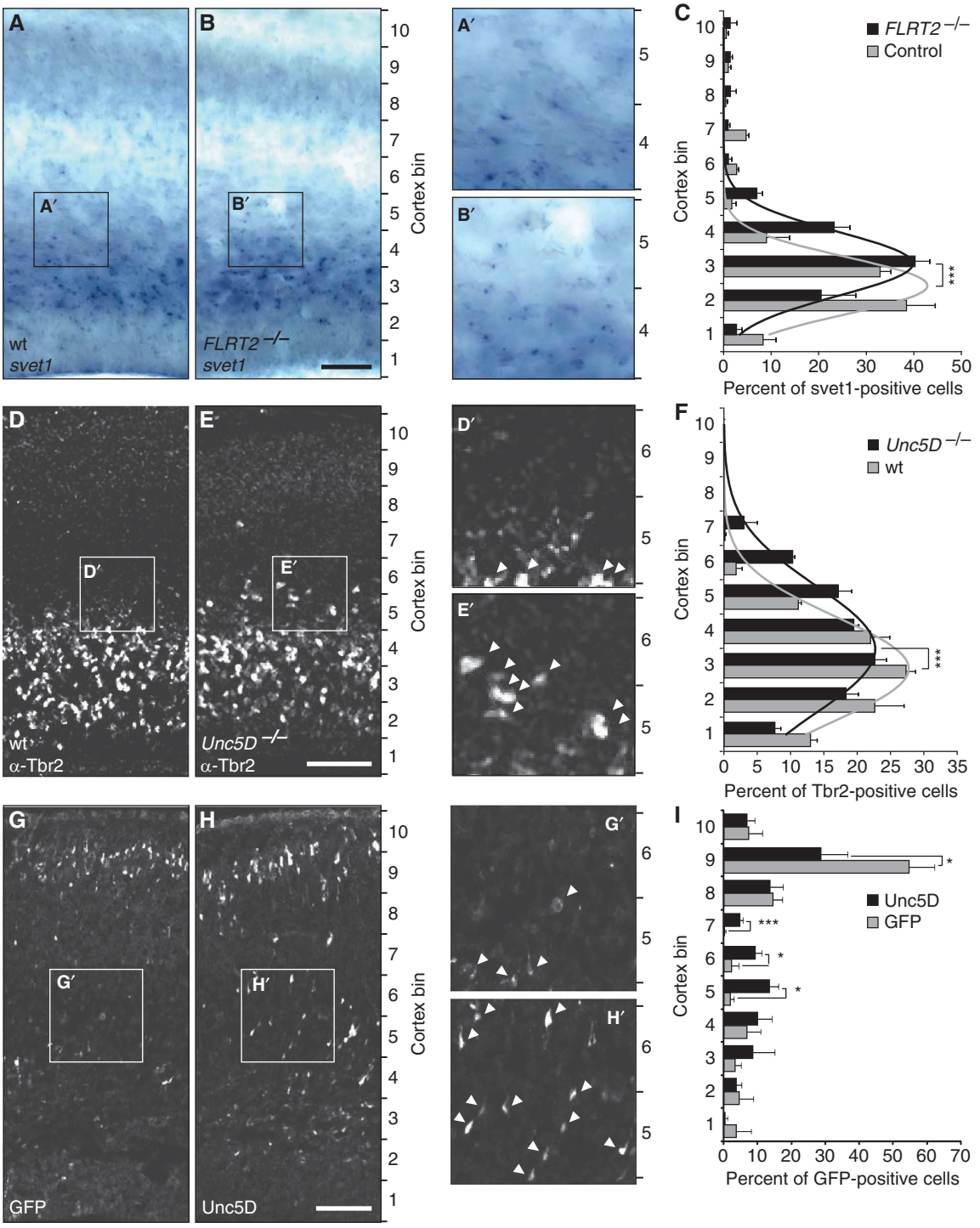

Figure 8 Acceleration of radial migration in FLRT2$^{-/-}$ and Unc5D$^{-/-}$ mice. (**A–C**) *svet1* ISH on coronal sections of E15.5 cortex. (**A**, **B**) Representative images of wt and *FLRT2*$^{-/-}$ sections. (**C**) Cortex was divided into 10 bins of 150 μm width and the percentages of svet1 + cells were plotted. The distribution mean of svet1-positive cells in *FLRT2*$^{-/-}$ mice was significantly shifted up by 0.6 bins (control, 2.436 ± 0.060; *FLRT2*$^{-/-}$, 3.074 ± 0.066; mean ± s.e.m.). $P<0.0001$, sum-of-square F-test, $n=3$ animals where every n was obtained from the average of 1–3 sections per animal. (**D–F**) Tbr2 staining on coronal sections of E15.5 cortex. (**D**, **E**) Representative images of wt and *Unc5D*$^{-/-}$sections. (arrowheads; Tbr2 + cells). (**F**) Cortex was divided into 10 bins as above and the percentages of Tbr2 + cells were plotted. The distribution mean of Tbr2 + cells in *Unc5D*$^{-/-}$ mice was significantly shifted up by 0.55 bins (wt, 2.915 ± 0.078; *Unc5D*$^{-/-}$, 3.474 ± 0.090; mean ± s.e.m.). $P<0.0001$, sum-of-square F-test, $n=3$ animals where every n was obtained from the average of five sections per animal. (**G**, **H**) Overexpression of GFP or Unc5D in developing cortex. Representative coronal sections of E17.5 cortex after IUE at E13.5 with GFP (**G**) or Unc5D-IRES-GFP (**H**) (arrowheads; GFP + cells). (**I**) Cortex was divided into 10 bins as above and the percentages of GFP + cells were plotted. The distribution of GFP + cells is significantly reduced in upper bins (bin 9) and increased in lower bins (bins 5–7) in the Unc5D electroporated brains. *$P<0.05$, ***$P<0.001$, *t*-test, control $n=3$, Unc5D $n=4$ animals, where every n was obtained from the average of 3–4 sections analysed per animal. Scale bars: 100 μm.

highest in the upper layers, while FLRT2 expression was confined to deep layers (Figure 7N–P) and this topography was maintained postnatally (Supplementary Figure S6). The svet1 probe detected many migratory cells in the deep layers of the CP, which continued to show the condensed (nuclear) signal (Figure 7P′). The Unc5D probe detected few migratory cells with a condensed signal (Figure 7O′) and many cells in the SVZ and CP with a cytoplasmic signal (Figure 7O″). These expression patterns were compatible with the hypothesis that the shed FLRT2 ECDs may function at a distance to guide Unc5D-positive cells. Among the canonical Unc5 ligands of the Netrin family, only Netrin-4 was found to be expressed in the developing cortex and restricted to the VZ/SVZ regions (Supplementary Figure S6; Yin *et al*, 2000).

FLRT2 and Unc5D regulate cortical neuron migration in vivo

Next, we asked if FLRT2 in the CP could be the repulsive cue that causes Unc5D+ neurons to reside in the SVZ for a prolonged period prior to starting their migration to the CP between E18.5 and P2 (Tarabykin *et al*, 2001; Britanova *et al*, 2008). If this hypothesis were correct, ablation of FLRT2 or Unc5D should cause these cells to leave the SVZ prematurely. Although a fraction of mutants showed embryonic lethality due to cardiovascular problems (Muller *et al*, 2011), about 50% of FLRT2 mutants generally survived without any obvious phenotype until E15 (data not shown). Ablation of FLRT2 did not affect cortical layering and neuron viability and did not cause any obvious neuropathological problems (data not shown). To analyse the distribution of Unc5D+ cells in the *FLRT2*$^{-/-}$ mice, E15.5 brain sections were labelled with the svet1 ISH probe, the region between the VZ and the pial surface was divided into 10 equally sized bins and cell numbers were counted in each bin. The overall numbers of svet1-positive cells were not altered in *FLRT2*$^{-/-}$ mice (Supplementary Figure S7). To facilitate the analysis of the distribution of the whole svet1-positive cell population in the cortex, we modelled the data to a Gaussian fit by non-linear regression (see Materials and methods). The analysis revealed that the mean of the Gaussian fit in *FLRT2*$^{-/-}$ mice was shifted by 0.6 bins towards upper layers compared with controls (Figure 8C, $n=3$ mice per group, $P<0.0001$, sum-of-square F-test), suggesting that a subpopulation of Unc5D+ cells is influenced by the presence of FLRT2. Interestingly, total numbers and the distribution of Satb2-positive cells, which do not linger in the SVZ, was unchanged in *FLRT2*$^{-/-}$ mice (Supplementary Figure S7). The distribution of SVZ cells in *Unc5D*$^{-/-}$ brains could not be done with the svet1 probe. Instead, we used Tbr2 antibodies that detected a much larger population of SVZ cells (not only Unc5D+ cells). Normally, in midgestation embryos, Tbr2+ cells are confined to the SVZ and they are rarely found in the IZ or CP (Figure 8D). In *Unc5D*$^{-/-}$ brains, although the majority of Tbr2+ cells are located in the SVZ, we found a broader distribution of Tbr2+ cells towards the CP (Figure 8D–F). The Gaussian fit revealed a shift by 0.55 bins towards upper layers compared with controls (Figure 8F; $n=3$ mice per group, $P<0.0001$, sum-of-square F-test). The same Tbr2 analysis did not reveal a phenotype in *FLRT2*$^{-/-}$ brains (data not shown), possibly because the FLRT2-sensitive subpopulation of Unc5D+ cells is too small to be detected with Tbr2 staining. We conclude that the Tbr2 phenotype in the Unc5D$^{-/-}$ embryos is either independent of FLRT2 or an additive/synergistic phenotype of lack of FLRT2 and of another Unc5D ligand that remains to be identified. To complement our loss-of-function analysis, we over-expressed Unc5D by *in utero* electroporation (IUE) and followed the migration of these cells. Overexpression of Unc5D in E13.5 born neocortical cells delayed their migration and prevented them from entering the CP at E17.5 (Figure 8G and H). As the data of this experiment could not be reliably modelled by a Gaussian fit, single bins were compared. The numbers of Unc5D-expressing cells were reduced by half in upper bins and concomitantly increased in lower bins (Figure 8I). These cells were, however, not completely compromised to migrate and eventually reached the upper layer of CP at early postnatal stage P0 (data not shown). This effect was not related to an increase in cell death due to Unc5D overexpression (Supplementary Figure S7). Together, these findings suggest that FLRT2 represents an *in vivo* guidance cue that causes Unc5D+ cells to reside in the SVZ for a prolonged period of time before migrating to the CP.

Discussion

Here, we report that FLRT2 and FLRT3 act as repulsive guidance molecules for Unc5 receptor-expressing neurons. Binding studies and *in vitro* growth cone collapse assays revealed specific interactions between the ECDs of FLRT2 and Unc5D (and to lesser extent with Unc5B), and between FLRT3 and Unc5B receptors. All FLRT proteins undergo ECD cleavage by metalloproteases and cleaved ECDs can be visualized *in vivo*, suggesting non-cell autonomous functions independent of their respective ICDs. Moreover, we show that Unc5D and FLRT2 regulate the radial migration of a subset of cortical neurons *in vivo*.

Mouse Unc5B and Unc5D were recently identified as high-affinity interactors of *Xenopus* FLRT3 (Karaulanov *et al*, 2009) and *Zebrafish* Unc5B was shown to bind *Zebrafish* FLRT1b and FLRT3 (Sollner and Wright, 2009). Our own interaction screen revealed a high degree of binding specificity between mouse Unc5 and FLRT family proteins: FLRT2 bound most strongly to Unc5D and to a lesser extent to Unc5B; FLRT3 bound to Unc5B. High-affinity interactions correlated with functional cellular readouts: FLRT2-induced growth cone collapse was markedly reduced in *Unc5D*$^{-/-}$ cortical neurons compared with wild-type neurons; FLRT3-induced growth cone collapse was attenuated by Unc5B knockdown. The discrepancies between our binding affinities and published reports could arise from the fact that xFLRT3 was probed against mouse Unc5 proteins (Karaulanov *et al*, 2009). *Zebrafish* FLRTs are not highly homologous to mouse FLRTs and this may explain the different binding affinities to Unc5B (Sollner and Wright, 2009).

We found that the FLRT ECDs were shed by neurons *in vivo* raising the possibility that they may act as diffusible ligands for Unc5 receptors on opposing cells. In the cortex, where FLRT2 expression is restricted to the CP, we found an enrichment of the shed FLRT2 ECD in the SVZ+VZ regions where it can interact with the Unc5D+ cells located in the SVZ. Although we have not yet formally proven that the shed ECDs are biologically active, indirect evidence supports such a model. FLRT2-His, a monomeric recombinant protein with

a small epitope tag and of similar size as the shed ECD has growth cone collapsing activity. Unlike soluble ephrin-Fc proteins, which require preclustering to be functional (Stein *et al*, 1998), FLRT ECDs are functional without preclustering, suggesting that shed FLRT ECDs acquire an active conformation *in vivo*.

Using a combination of gain- and loss-of-function experiments in the mouse, we provide evidence that FLRT2 and Unc5D delay the initiation of migration of young neurons in the cortex. Later born cortical neurons have previously been shown to consist of at least two different subpopulations of cells that were characterized by expression of the markers Satb2 and Unc5D/Svet1 (Britanova *et al*, 2008). They also differ in migration behaviours. Satb2+ cells start their migration immediately after mitotic cycle exit and arrive in the CP early in development at E14.5–E15.5. Unc5D/Svet1 cells instead reside in the SVZ for at least 3–4 days and commence migration only after E17.5 to finally settle in the CP by P2. It is not known whether the pause of Unc5D/Svet1 cells in the SVZ is required for their normal development or whether they contribute to the microenvironment of the SVZ. Our results show that FLRT2 acts to prevent a subpopulation of Unc5D/Svet1 cells from premature departure from the SVZ. To initiate migration, Unc5D+ cells appear to downregulate Unc5D expression, which allows them to traverse the FLRT2-positive layers. Once the cells arrive in upper cortical layers, which are FLRT2 negative, Unc5D expression reappears (see model in Supplementary Figure S8).

Considering the high binding affinity of FLRT2 to Unc5D and the strong repulsive effect of FLRT2 on migrating cells, the defect in cortical migration in the respective genetic mutants seems rather modest. The other family members FLRT3 and Unc5B are partially co-expressed with FLRT2/Unc5D, raising the possibility that they can partially compensate for the lack of FLRT2/Unc5D. Generation and analysis of double knockouts are in progress to test these hypotheses. Among the secreted Netrins, only Netrin-4 is expressed in the VZ and SVZ region of the developing cortex. This expression pattern would be most consistent with a role of Netrin-4 pushing Unc5D+ cells towards the CP. If this scenario was correct, loss of Unc5D should delay migration, whereas overexpression of Unc5D should accelerate migration. However, the converse is true; loss of Unc5D accelerates migration and overexpression of Unc5D delays migration. We therefore conclude that Netrin-4 does not modulate the migration of Unc5D+ cells towards the CP. It is possible that Netrin-4 in the VZ serves to prevent Unc5D+ cells from undergoing apoptosis (Takemoto *et al*, 2011).

Most genes implicated in radial migration of cortical neurons encode intrinsic factors that affect the cytoskeleton (Heng *et al*, 2008; Jaglin and Chelly, 2009). Few soluble extrinsic cues that influence cortical pyramidal neuron migration have been described, including Reelin (Soriano and Del Rio, 2005), Sema3A (Polleux *et al*, 2000; Chen *et al*, 2008) and SPARC-like-1 (Gongidi *et al*, 2004). It is interesting to note that Sema3A mRNA transcripts are found in the CP in a pattern similar to FLRT2, and that Neuropilin-1 (NP1) expression is highest in the SVZ similar to Unc5D (Polleux *et al*, 2000; Chen *et al*, 2008). Sema3A is a chemoattractant for newborn NP1+ cortical neurons towards upper layers (Chen *et al*, 2008). In addition, Sema3A controls the polarized growth of these neurons by repelling their axon and attracting their apical dendrites (Polleux *et al*, 2000). It is possible that repulsive FLRT2 and attractive Sema3A signals cooperate in guiding projection neurons to their appropriate cortical layers. Unc5D+ migrating cells downregulate Unc5D expression so that FLRT2 signalling is silenced. The Sema3A signal may become dominant and cells can follow the chemoattractant to migrate towards upper layers. To demonstrate this, further experiments are needed.

Materials and methods

Generation of FLRT1, FLRT2 and Unc5D knockout and FLRT3^{lx} conditional alleles

Mutant mice were generated by homologous recombination in ES cells using a replacement-type targeting vector (see Supplementary Figures S1, S2 and S4). ES cell cultures, electroporation and selection were carried out according to the standard protocols. Screening and homologous recombination on both arms of the constructs was assessed by Southern blots in the targeted ES cells. Germline transmission was achieved with at least two independent ES cell clones for each gene. The *FLRT3^{lx}* allele was crossed to the nervous system-specific Nestin-Cre line (Tronche *et al*, 1999). Most of the experiments were carried out in a mixed 129/SvEv × C57BL/6 background. The *FLRT2*$^{-}$ mice were maintained in both C57BL/6 and CD1 background.

Immunostaining

For tissue treatments see Supplementary data. The following antibodies were used: anti-Tbr2 (1/200; Abcam), anti-SatB2 (1/5; Abcam), anti-GFP (1/500; Rockland), anti-active caspase-3 (1:500; BD Pharmigen) and anti-FLRT2 (1/40; R&D Systems). Images were acquired using an epifluorescence microscope (Axioplan2, Carl Zeiss MicroImaging) equipped with a digital camera (SpotRT; Diagnostic Instruments) and analysed using the Metamorph software (Visitron). For Tbr2 and SatB2 staining, 5 μm stacks (1 μm steps) were acquired with a Leica SP2 confocal laser scanning microscope. For the analysis of cell distribution in the cortex, the distance from ventricle to pia was divided into 10 equal sized bins of 150 μm width. All Tbr2+, Satb2+, GFP+ or *svet1*+ cells were counted.

Stripe assay

For the stripe assay, 50 μg/ml of recombinant control Fc and FLRT2/3 ECD-Fc proteins were preclustered with Alexa488-conjugated anti-hFc antibody (Invitrogen) in PBS for 30 min. For competition assays, preclustered Fc and FLRT2/3 ECD-Fc were preincubated with 50 μg/ml of recombinant control Fc or Unc5 ECD-Fc for 45 min. Proteins were injected into matrices (90 μm width) placed on 60 mm dishes (Knoll *et al*, 2007), resulting in the first green-fluorescent stripes. After 30 min incubation at 37°C, dishes were washed with PBS and matrices were carefully removed. The dishes were further coated with 50 or 100 μg/ml (for competition assays) of Fc protein preclustered with anti-hFc (no fluorescent dye) for 30 min at 37°C and, after washing three times with PBS, with 20 μg/ml of laminin for 1 h at 37°C. Hippocampal or cortical neurons from E15.5 mice were dissociated and cultured for 24 h on the stripes. Neurons were fixed with 4% sucrose/4% PFA in PBS for 20 min at RT, washed and incubated with mouse monoclonal anti-Tau1 antibody (Chemicon) after permeabilization in 0.3% Triton X-100/PBS. Cy3 anti-mouse IgG secondary antibody (Jackson) was used to visualize the Tau1 signal. After taking the images as above, axons and cell soma were separated and digitalized using Adobe Photoshop. The images were further separated into two parts (on green or black stripes). The total numbers of Tau1+ pixels were quantified using Image J. For time-lapse movies, dishes were incubated at 37°C with 5% CO_2 in the humid chamber of an inverted microscope. Phase-contrast pictures were obtained every 15 min from 2 to 14 h after plating the cells. The movies were created and merged with the fluorescent channel using Metamorph software (Visitron, Puchheim, Germany).

Biochemistry and transient transfection experiments in HEK293 cells

Brain or cell lysates were obtained as previously described (Egea *et al*, 2005). For the microdissection experiments, E15.5 thick (350 μm) coronal sections of the cortex were cut along the IZ to mechanically separate the SVZ + VZ from the CP + MZ. HEK293T cells were transiently transfected using FuGENE6 (Roche). Metalloprotease inhibitors (TAPI-0, TAPI-I and GM6001; Calbiochem) are treated for 1 day in the indicated experiments. Glycoproteins were pulled down from 100 to 1000 μg of protein lysate or culture media using wheat germ agglutinin (lectin) agarose beads (Sigma). In the indicated experiments, recombinant *N*-glycosidase (Roche) was added after lectin pull down for overnight at 37°C. Western blots in total cell lysates or lectin pull downs were performed as indicated: anti-FLRT1/2/3 ECD (1/1000; R&D Systems), anti-FLRT1-ICD (1/1000; our own serum 1160), anti-FLRT2-ICD (1/200; Santa Cruz), anti-FLRT3-ICD (1/1000; our own serum 1134), anti-EphA4 mAb (anti-Sek 1/2000; Becton Dickinson Biosciences, San Jose, CA); anti-tubulin (1/50000; Sigma); anti-BOC (1/500; R&D Systems); anti-c-myc (1/2000; hybridoma 9E10 supernatant); anti-His (1/1000; Santa Cruz); anti-Unc5B (1/1000; R&D Systems); anti-Pax6 (1/200; Covance).

Statistical analysis

Statistical significance was determined using unpaired, two-tailed Student's *t*-tests in Microsoft Excel. For stripe assays, statistical significance was determined using one-way ANOVA and Tukey's *post hoc* test with the Prism version 5 (Graphpad Software, San Diego, CA). The non-linear regression for Gaussian fit was performed by a least-squares-fit with the Prism 5 software. The reliability of the model was validated by evaluating the residuals plot, replicate test, plausibility of best-fit values, 95% confidence intervals, width of confidence bands, R^2 values and sum-of-squares values. Statistical significance for the Gaussian fit was determined using sum-of-square F-test in Prism 5. All values in the text and in the figure legends indicate mean + s.e.m.

AP-binding assay

The entire ECD region of FLRT1, FLRT2 or FLRT3 was subcloned into pcDNA3.AP. At 24 h after transfection of HEK293T cells, the media was changed to OptiMEM + 2% FBS + 1 mM $CaCl_2$ and conditioned for 5 DIV. The activity and concentration of the recombinant protein in the media was estimated by using the AP substrate *p*-nitrophenylphosphate (Sigma) and Coomassie staining after SDS–PAGE gel electrophoresis, respectively. For the binding assays, HEK293T cells were transfected in poly-L-lysine-coated P48 or P24 well plates with the indicated constructs. After 24–36 h, the cells were incubated with the conditioned AP media (~250 nM of recombinant protein) for 1 h at room temperature and then washed with TBS containing 0.5% BSA. Cells were incubated for 1 h in AP buffer (50 mM Tris pH 9.5; 2 mM $MgCl_2$; 100 mM NaCl) containing naphtol FAST Red and then fixed with 4% PFA for imaging. Alternatively, cells were incubated with *p*-nitrophenylphosphate and analysed by absorbance at 405 nm after 60–90 min of reaction. Background activity in non-transfected cells was subtracted.

Supplementary data

Supplementary data are available at *The EMBO Journal* Online (http://www.embojournal.org).

Acknowledgements

We thank V Beilinson for making the Unc5D targeting construct; P Mehlen, L Hinck, T Iwata and ER Fearon for providing valuable reagents; E Stein for sharing reagents, unpublished observations and for discussions; G Seyit, L Gaitanos, J Bailey, K Yamagishi, C Martinez, C Gebhardt, M Fritz, R Sanchez, M Boesl and M Rodriguez, the Max Planck Transgenic and Mouse Facilities for excellent technical support. SY was supported by Mochida Memorial Foundation for Medical and Pharmaceutical Research, Japan Society for Promotion of Science and an EMBO long-term postdoctoral fellowship. JE holds a Ramon y Cajal contract from the Spanish Ministerio de Ciencia e Innovacion. This work was in part funded by the Max Planck Society (to RK and VT), by the Deutsche Forschungsgemeinschaft (SFB665 and Heisenberg Program to VT) and by the Generalitat de Catalunya (SGR740) and Ministerio de Ciencia e Innovación (BFU2010-18055) (to JE).

Author contributions: SY, FH, D.dT and JE designed, performed and analysed most of the biochemical, *ex vivo* and *in vivo* experiments. KH and TY designed, performed and analysed the growth cone collapse assays implicating Unc5B. MS, EK and VT designed, performed and analysed the *in utero* electroporations, provided the $Unc5D^{-/-}$ model and aided in the interpretation of data. MB helped with the stripe assays. RK and JE co-supervised the project, designed experiments and co-wrote the manuscript with SY and FH.

Conflict of interest

The authors declare that they have no conflict of interest.

References

Ackerman SL, Kozak LP, Przyborski SA, Rund LA, Boyer BB, Knowles BB (1997) The mouse rostral cerebellar malformation gene encodes an UNC-5-like protein. *Nature* **386:** 838–842

Bottcher RT, Pollet N, Delius H, Niehrs C (2004) The transmembrane protein XFLRT3 forms a complex with FGF receptors and promotes FGF signalling. *Nat Cell Biol* **6:** 38–44

Bradford D, Cole SJ, Cooper HM (2009) Netrin-1: diversity in development. *Int J Biochem Cell Biol* **41:** 487–493

Britanova O, de Juan Romero C, Cheung A, Kwan KY, Schwark M, Gyorgy A, Vogel T, Akopov S, Mitkovski M, Agoston D, Sestan N, Molnar Z, Tarabykin V (2008) Satb2 is a postmitotic determinant for upper-layer neuron specification in the neocortex. *Neuron* **57:** 378–392

Budagian V, Bulanova E, Orinska Z, Duitman E, Brandt K, Ludwig A, Hartmann D, Lemke G, Saftig P, Bulfone-Paus S (2005) Soluble Axl is generated by ADAM10-dependent cleavage and associates with Gas6 in mouse serum. *Mol Cell Biol* **25:** 9324–9339

Burgess RW, Jucius TJ, Ackerman SL (2006) Motor axon guidance of the mammalian trochlear and phrenic nerves: dependence on the netrin receptor Unc5c and modifier loci. *J Neurosci* **26:** 5756–5766

Chen G, Sima J, Jin M, Wang KY, Xue XJ, Zheng W, Ding YQ, Yuan XB (2008) Semaphorin-3A guides radial migration of cortical neurons during development. *Nat Neurosci* **11:** 36–44

Egea J, Erlacher C, Montanez E, Burtscher I, Yamagishi S, Hess M, Hampel F, Sanchez R, Rodriguez-Manzaneque MT, Bosl MR, Fassler R, Lickert H, Klein R (2008) Genetic ablation of FLRT3 reveals a novel morphogenetic function for the anterior visceral endoderm in suppressing mesoderm differentiation. *Genes Dev* **22:** 3349–3362

Egea J, Nissen UV, Dufour A, Sahin M, Greer P, Kullander K, Mrsic-Flogel TD, Greenberg ME, Kiehn O, Vanderhaeghen P, Klein R (2005) Regulation of EphA 4 kinase activity is required for a subset of axon guidance decisions suggesting a key role for receptor clustering in Eph function. *Neuron* **47:** 515–528

Geling A, Steiner H, Willem M, Bally-Cuif L, Haass C (2002) A gamma-secretase inhibitor blocks Notch signaling *in vivo* and causes a severe neurogenic phenotype in zebrafish. *EMBO Rep* **3:** 688–694

Gongidi V, Ring C, Moody M, Brekken R, Sage EH, Rakic P, Anton ES (2004) SPARC-like 1 regulates the terminal phase of radial glia-guided migration in the cerebral cortex. *Neuron* **41:** 57–69

Hata K, Kaibuchi K, Inagaki S, Yamashita T (2009) Unc5B associates with LARG to mediate the action of repulsive guidance molecule. *J Cell Biol* **184:** 737–750

Heng JI, Nguyen L, Castro DS, Zimmer C, Wildner H, Armant O, Skowronska-Krawczyk D, Bedogni F, Matter JM, Hevner R, Guillemot F (2008) Neurogenin 2 controls cortical neuron migration through regulation of Rnd2. *Nature* **455:** 114–118

Jaglin XH, Chelly J (2009) Tubulin-related cortical dysgeneses: microtubule dysfunction underlying neuronal migration defects. *Trends Genet* **25:** 555–566

Karaulanov E, Bottcher RT, Stannek P, Wu W, Rau M, Ogata S, Cho KW, Niehrs C (2009) Unc5B interacts with FLRT3 and Rnd1 to modulate cell adhesion in Xenopus embryos. *PLoS One* **4:** e5742

Karaulanov EE, Bottcher RT, Niehrs C (2006) A role for fibronectin-leucine-rich transmembrane cell-surface proteins in homotypic cell adhesion. *EMBO Rep* **7:** 283–290

Knoll B, Weinl C, Nordheim A, Bonhoeffer F (2007) Stripe assay to examine axonal guidance and cell migration. *Nat Protoc* **2:** 1216–1224

Kruger RP, Lee J, Li W, Guan KL (2004) Mapping netrin receptor binding reveals domains of Unc5 regulating its tyrosine phosphorylation. *J Neurosci* **24:** 10826–10834

Lacy SE, Bonnemann CG, Buzney EA, Kunkel LM (1999) Identification of FLRT1, FLRT2, and FLRT3: a novel family of transmembrane leucine-rich repeat proteins. *Genomics* **62:** 417–426

Lefebvre T, Planque N, Leleu D, Bailly M, Caillet-Boudin ML, Saule S, Michalski JC (2002) O-glycosylation of the nuclear forms of Pax-6 products in quail neuroretina cells. *J Cell Biochem* **85:** 208–218

Leonardo ED, Hinck L, Masu M, Keino-Masu K, Ackerman SL, Tessier-Lavigne M (1997) Vertebrate homologues of C. elegans UNC-5 are candidate netrin receptors. *Nature* **386:** 833–838

Maretto S, Muller PS, Aricescu AR, Cho KW, Bikoff EK, Robertson EJ (2008) Ventral closure, headfold fusion and definitive endoderm migration defects in mouse embryos lacking the fibronectin leucine-rich transmembrane protein FLRT3. *Dev Biol* **318:** 184–193

Mehlen P, Furne C (2005) Netrin-1: when a neuronal guidance cue turns out to be a regulator of tumorigenesis. *Cell Mol Life Sci* **62:** 2599–2616

Moore SW, Tessier-Lavigne M, Kennedy TE (2007) Netrins and their receptors. *Adv Exp Med Biol* **621:** 17–31

Muller PS, Schulz R, Maretto S, Costello I, Srinivas S, Bikoff E, Robertson E (2011) The fibronectin leucine-rich repeat transmembrane protein Flrt2 is required in the epicardium to promote heart morphogenesis. *Development (Cambridge, England)* **138:** 1297–1308

Ogata S, Morokuma J, Hayata T, Kolle G, Niehrs C, Ueno N, Cho KW (2007) TGF-beta signaling-mediated morphogenesis: modulation of cell adhesion via cadherin endocytosis. *Genes Dev* **21:** 1817–1831

Polleux F, Morrow T, Ghosh A (2000) Semaphorin 3A is a chemoattractant for cortical apical dendrites. *Nature* **404:** 567–573

Rakic P (1988) Specification of cerebral cortical areas. *Science (New York, NY)* **241:** 170–176

Robinson M, Parsons Perez MC, Tebar L, Palmer J, Patel A, Marks D, Sheasby A, De Felipe C, Coffin R, Livesey FJ, Hunt SP (2004) FLRT3 is expressed in sensory neurons after peripheral nerve injury and regulates neurite outgrowth. *Mol Cell Neurosci* **27:** 202–214

Sasaki S, Tabata H, Tachikawa K, Nakajima K (2008) The cortical subventricular zone-specific molecule Svet1 is part of the nuclear RNA coded by the putative netrin receptor gene Unc5d and is expressed in multipolar migrating cells. *Mol Cell Neurosci* **38:** 474–483

Sollner C, Wright GJ (2009) A cell surface interaction network of neural leucine-rich repeat receptors. *Genome Biol* **10:** R99

Soriano E, Del Rio JA (2005) The cells of cajal-retzius: still a mystery one century after. *Neuron* **46:** 389–394

Stein E, Lane AA, Cerretti DP, Schoecklmann HO, Schroff AD, Van Etten RL, Daniel TO (1998) Eph receptors discriminate specific ligand oligomers to determine alternative signaling complexes, attachment, and assembly responses. *Genes Dev* **12:** 667–678

Takemoto M, Hattori Y, Zhao H, Sato H, Tamada A, Sasaki S, Nakajima K, Yamamoto N (2011) Laminar and areal expression of Unc5d and its role in cortical cell survival. *Cereb Cortex* (advance online publication, 7 January 2011; doi:10.1093/cercor/bhq265)

Tarabykin V, Stoykova A, Usman N, Gruss P (2001) Cortical upper layer neurons derive from the subventricular zone as indicated by Svet1 gene expression. *Development (Cambridge, England)* **128:** 1983–1993

Tronche F, Kellendonk C, Kretz O, Gass P, Anlag K, Orban PC, Bock R, Klein R, Schutz G (1999) Disruption of the glucocorticoid receptor gene in the nervous system results in reduced anxiety. *Nat Genet* **23:** 99–103

Tsuji L, Yamashita T, Kubo T, Madura T, Tanaka H, Hosokawa K, Tohyama M (2004) FLRT3, a cell surface molecule containing LRR repeats and a FNIII domain, promotes neurite outgrowth. *Biochem Biophys Res Commun* **313:** 1086–1091

Vielmetter J, Stolze B, Bonhoeffer F, Stuermer CA (1990) *In vitro* assay to test differential substrate affinities of growing axons and migratory cells. *Exp Brain Res* **81:** 283–287

Walther C, Gruss P (1991) Pax-6, a murine paired box gene, is expressed in the developing CNS. *Development (Cambridge, England)* **113:** 1435–1449

Yin Y, Sanes JR, Miner JH (2000) Identification and expression of mouse netrin-4. *Mech Dev* **96:** 115–119